ORIENTAL JOURNAL OF CHEMISTRY
An International Open Access, Peer Reviewed Research Journal
www.orientjchem.org
ISSN: 0970-020 X
CODEN: OJCHEG
2025, Vol. 41, No.(2):
Pg. 506-517

Synthesis, Characterization and Activity Evaluation of Sulphate Modified Cu-MOF Catalyst for the Valorization of Glycerol to Solketal

VENNELA ALUVALA[1], BALAKRISHNA MATKALA[1], SWAROOPA CHILKAMARRI[1], VIJAYALAXMI BURRI[1], SASIKUMAR BOGGALA[2], ANJANEYULU CHATLA[2], SREEDHAR INKOLLU[3] and HARI PADMASRI AYTAM[1]*

[1]Department of Chemistry, University College of Science, Osmania University, Hyderabad-500 007, Telangana, India.
[2]Catalysis and Fine Chemicals Department, CSIR-Indian Institute of Chemical Technology, Hyderabad-500 007, Telangana, India.
[3]Department of Chemical Engineering, Birla Institute of Technology and Science, Pilani, Hyderabad 500 078, Telangana, India.
*Corresponding author E-mail: ahpadmasri@osmania.ac.in; ahpadmasri@gmail.com

http://dx.doi.org/10.13005/ojc/410220

(Received: February 18, 2025; Accepted: March 31, 2025)

ABSTRACT

Sulphated Cu- trimesic acid metal organic framework (MOF) catalysts with varying amounts of sulphate were synthesized and evaluated for glycerol acetalization to solketal under ambient conditions. A significantly high performance was exhibited by sulphated Cu-BTC MOFs in comparison to the parent Cu-BTC. The Cu-MOF based catalysts were analysed by XRD, BET-SA, TGA, FT-IR, Raman spectroscopy, SEM, XPS and Ex-situ pyridine adsorbed IR studies (Py-IR) to have insight into their properties that explain their glycerol acetalization activity. The high surface area of MOFs, role played by Lewis acid sites on the catalyst surface may be regarded as the riders for the enhanced formation of solketal over these catalysts. The Cu-BTC catalyst recovered after five cycles of reaction run revealed consistent activity under similar experimental conditions.

Keywords: Cu-BTC MOF, Sulphated, Glycerol acetalization, Lewis acid sites, Ex-situ Py-IR.

INTRODUCTION

MOFs are versatile crystalline, porous and 3-dimensional network materials of metal clusters ligated to organic linkers. The voids in between the metal ions and organic linkers form pores that are responsible for high pore volume and large surface area of MOFs. MOFs cover a wide range of hybrid compounds with tunable structures, unique properties due to variable metal ions and organic ligand molecules[1-2]. Owing to these tunable properties they are highly potential and provide great opportunities in applications such as separation, sensing and catalysis[3-7]. Recently,

MOFs were investigated for various heterogeneous catalytic organic transformations such oxidation, hydrogenation and acid-base catalyzed reactions[8-12]. They were reported as Lewis-acid catalysts in reactions such as acetalization of aldehydes, Knoevenagel condensation, Friedlander synthesis and reduction reactions[13-16]. Cu-MOFs are reported to have good thermal stability along with reversible adsorption-desorption properties and known to catalyze a variety of reactions[17].

A surge in the utilization of renewable energy sources is seen over last decades, with considerable increase in biodiesel production owing to continuous depletion of non-renewable conventional resources and to environmental concerns[18,19]. The biodiesel production by the base-catalyzed transesterification of triglycerides from vegetable oils also generates the by-product, glycerol in 10 wt.%[20]. This makes the process economically unviable with expensive large scale purification processes involved[21,22]. Thus, it is inevitable to devise processes for the value addition of glycerol in transforming it into useful products[23].

Several value-added chemicals such as polymers, surfactants, bio-solvents and glycerol derivatives can be obtained from the crude-glycerol transformation[24-27]. Compounds derived from glycerol have been recognized to exhibit improved physico-chemical properties when blended with diesel or petrol with reduced particulate emissions[28-32].

The products of glycerol reaction with acetic acid or t-butanol are highly valuable compounds as bio-additives of fuels[33-36]. Solketal is one other such compound that has great potential as a fuel additive to improve the performance of fossil-based fuels i.e., diesel and gasoline. Its use is also reported to have increased octane index, reduce viscosity, improved flashpoint and also used to reduce gum formation[32,37-39].

Synthesis of Solketal via acid-catalyzed reactions involve homogeneous catalysts that are highly corrosive and environmentally unfriendly processes[40]. These processes involve serious drawbacks with a tedious workup and extensive separation from products generating large amounts of effluents and residues that have to be neutralized before their safe disposal into the environment[41].

Cost effective and selective solid acid heterogeneous catalysts such as metal oxides, sulfonic acid resins, zeolite, supported metal/metal oxide catalysts, mesoporous silica-based catalysts are reported as alternatives to homogenous catalysts to circumvent their drawbacks[42-44]. The challenges faced by these systems involve active phase leaching leading to loss of solid-supported catalysts' activity. However, reports on AlF_3, zeolite catalysts viz., Hβ, metal incorporated modified MCM-41, SBA-15 catalysts showed significant and stable activity[45-51].

The present work is the utilization of sulphate modified Cu-MOFs for the selective synthesis of solketal from glycerol at ambient conditions. Variable amounts of sulphate loaded Cu-MOF catalysts were tested for this reaction under differential reaction conditions to optimize the parameters in achieving the best yield of solketal possible over these catalysts. The catalysts were also evaluated for reusability for about 5 cycles of reaction and found to exhibit stable activity and consistent selectivity of the desired product formation.

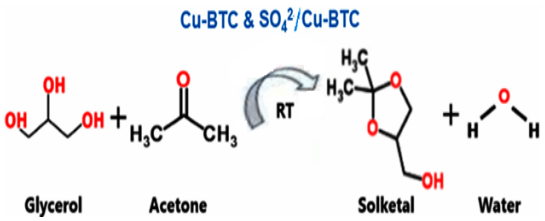

Scheme 1. Glycerol Acetalization over sulphated Cu-BTC MOF catalysts

MATERIALS AND METHODS

Materials used

All the chemicals obtained from Sigma-Aldrich, viz; copper nitrate hexa hydrate, trimesic acid (BTC), dimethyl formamide (DMF), ethanol, Glycerol (99%) and Acetone (99%) were used as purchased in the current work.

Cu-BTC MOF and Sulphated Cu-BTC MOFs Synthesis

Cu-BTC MOF is prepared by the mixing of two solutions A and B with thorough mixing on a magnetic stirrer. The solution-A is obtained by dissolving BTC (0.0234 mol) in EtOH while $Cu(NO_3)_2.3H_2O$ (0.0466 mol) in 1:1 ratio of DMF (25 mL) and deionized water (25 mL) is taken as solution-B. The mixture obtained thus from A and B

is autoclaved for hydrothermal treatment at 85°C for 24 hours. Then the mother liquor obtained after hydrothermal treatment is decanted and washed thoroughly with DMF and ethanol. The resultant solid is dried at 170°C in a vacuum oven for 6 h and finally fine deep blue crystals of Cu-MOF were obtained[9].

Sulphated Cu-BTC catalysts were prepared with varying concentrations (0.1 N, 0.2 N, 0.3N, 0.5 N and 1N) of H_2SO_4 by impregnating required amounts on 1 g of the parent Cu-BTC separately at 25°C with stirring for 2 hours. The material was then washed thoroughly using deionized water and dried in an oven completely at 100°C for overnight[9]. The resultant sulphated catalysts were labelled as 0.1S-Cu-MOF, 0.2S-Cu-MOF, 0.3S-Cu-MOF, 0.5S-Cu-MOF and 1S-Cu-MOF respectively.

Characterization of the prepared catalysts

A Rigaku miniplex diffractometer was used for XRD analysis that was operated at 40V and 15mA with Cu-Kα (1.5406 Å) as source of radiation recorded in the range of 2θ = 5 to 80°. A Varian 660-IR spectrometer was used for recording IR and Py-adsorbed IR spectra. Ex-situ Py-IR adsorption studies of the samples were done by exposure of samples to pyridine vapours until the surface is saturated and excess amount is flushed out in Ar at 150°C for one hour. Later from the obtained spectra, spectrum of the unadsorbed sample was subtracted to obtain the signals corresponding to pyridinium ion over Bronsted acid sites at ~1540 cm^{-1} and at ~1450 cm^{-1} due to coordinated pyridine over Lewis acid site. Perkin Elmer STA 6000 was used to record thermograms from 303 to 973 K typically by heating a sample at a ramp of 10 $Kmin^{-1}$ in N_2. Microscopic analysis & EDS spectra of the samples were obtained from a JEOL JSM-6010/LA microscope. Surface areas of catalysts were measured by recording N_2 sorption isotherms on a Micrometric ASAP 2010 surface analyzer at -196°C to fit in BET-equation. Mg K radiation was used for XPS analysis of samples on KRATOS-AXIS 165 instrument. Raman spectra were recorded using a 633 nm He–Ne laser source with the scattered light analysed using HORIBA JOBIN YVON HR800, Japan.

Acetalization activity tests

Acetalization activity of glycerol to solketal was tested in a liquid phase batch type reactor kept under stirring using a magnetic stirrer at ambient reaction conditions. The various parameters such as catalyst amount, reactants mole ratio, time on stream and catalyst reusability studies were studied to optimize the reaction conditions for obtaining best possible yield of the desired product. Excess of acetone taken here acts as both acetalization agent as well as the solvent and is reported to favour the yields of solketal by enhancing the conversion of glycerol as it increases the polarity of the reaction mixture[48]. In this regard mole ratio variation of acetone to glycerol is done by maintaining glycerol content constant while varying the amount of acetone alone. The reaction mixture was analysed from time to time by drawing small amounts, centrifuging it to remove the catalyst particles before injecting into a Gas Chromatograph instrument of Varian CP-3800 make containing a flame ionization detector and a ZBwax capillary column. The products were established by injecting the authentic compounds of the expected products viz., solketal and dioxan product and by confirmation using GC-MS analysis. The catalyst reuse studies were done by centrifugation of reaction mixture to remove catalyst which was then washed thoroughly with water several times and with acetone also. Then the catalyst was oven dried for 2-3 h at 100°C before it is used for next cycle of reaction run. This process is repeated for 4 more times. The equations below are used to calculate the glycerol conversion and selectivity to solketal:

$$Conversion\ (\%) = \frac{No.of\ initial\ moles\ of\ glycerol - No.of\ final\ moles\ of\ glycerol}{No.of\ initial\ moles\ of\ glycerol}$$

$$Selectivity\ of\ Solketal\ (\%) = \frac{moles\ of\ Solketal\ formed}{Moles\ of\ glycerol\ converted} \times 100$$

$$Rate_{Solketal} = \frac{Yield\ of\ solketal \times moles\ of\ glycerol\ feed}{amount\ of\ catalyst(g) \times time(h)}$$

RESULTS AND DISCUSSION

X-ray Diffraction Analysis

X-ray diffractograms of the as synthesized Cu-BTC MOF and the sulphated Cu-BTC MOFs are presented in Fig. 1. The parent MOF is represented in Fig. 1a. The diffractograms indicate the formation of crystalline Cu-BTC MOF phased in all and the structure remained intact after sulphation also[52,53]. The presence of 2θ values of 6.6°, 9.44°, 11.76°, 13.71°, 15.14°, 16.73°, 17.16°, 19.23°, 25.92°, and 28.92° correspond to the miller indices (2 0 0), (2 2 0), (2 2 2), (4 0 0), (3 3 1), (4 2 2), (5 5 1), (4 4 0), (7 3 1) and (7 51) respectively indicate the Cu-BTC MOF phase as per the JCPDS no. 00-062-118354. The major peak observed at 11.76° is the most intensive shows the high crystallinity of the MOF material while the presence of Cu_2O, CuO phases is evidenced from the weak peaks of low intensities in the range of 35.4° to 43.0°. Formation of these phases

is reported due to the high temperature used in the synthesis of Cu-BTC MOFs[52,53]. A slight decrease in the crystallinity can be noticed with increase in the sulphate loading and the same may be established from the decreased crystallite size of the samples with the broadening of the peaks. The crystallite sizes of the catalysts calculated using Scherrer equation are displayed in Table 1 which support the decrease in crystallite size with sulphate loading as seen from the broadening of the peaks in diffractograms.

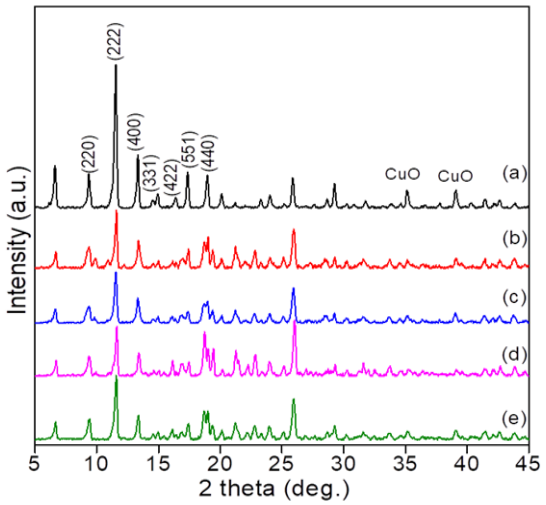

Fig. 1. X-ray diffraction profiles of (a) Cu-MOF, (b) 0.1S-Cu-MOF, (c) 0.2S-Cu-MOF, (d) 0.3S-Cu-MOF, (e) 0.5S-Cu-MOF

Table 1: Physico-chemical features of Cu-MOF catalysts

Catalyst	BET-SA (m^2g^{-1})	[a]Crystallite Size (nm)	[b]ILewis/IBronsted
Cu-MOF	1099	13.1	0.26
0.1S Cu-MOF	892	10.2	0.52
0.2S Cu-MOF	785	8.6	0.75
0.3S Cu-MOF	705	7.8	0.93
0.5S Cu-MOF	658	4.3	1.23
1S Cu-MOF	620	3.4	1.36

[a]XRD; [b]Ex-situ Py-IR

BET-Surface area

The N_2 sorption isotherms of Cu–BTC exhibited type–I isotherm indicating the predominant presence of micropores in the structure. The specific surface area of Cu-MOF synthesized were high as expected of the MOFs in general as seen from Table 1. Sulphation of Cu-BTC resulted in decrease in the surface area probably due to pore blockage by the sulphate groups. However, surface areas of the sulphated samples are yet quite higher compared to the conventional metal oxide supported, zeolite or mesoporous silica-based catalysts that makes MOF materials very unique and advantageous for the synthesis of desired products via heterogenous catalytic routes. The microporous and microcrystalline characteristics with good pore volume of these materials are also noteworthy in this regard.

Morphological studies

SEM/EDX

The morphological and textural features were analysed by SEM and EDX given in Fig. 2 (a) and (b) and these images of the synthesized cubic crystals of MOF exhibit octahedral and cubo-octahedral particle morphology. The particles almost retained their morphology after sulphation also (Fig. 2c). The EDX spectrum confirms the elements present in Cu-BTC MOF (fig. 6B), viz., Cu, C and O while that of 0.5S-Cu-MOF being the sulphated sample additionally indicated the presence of S in desired proportions.

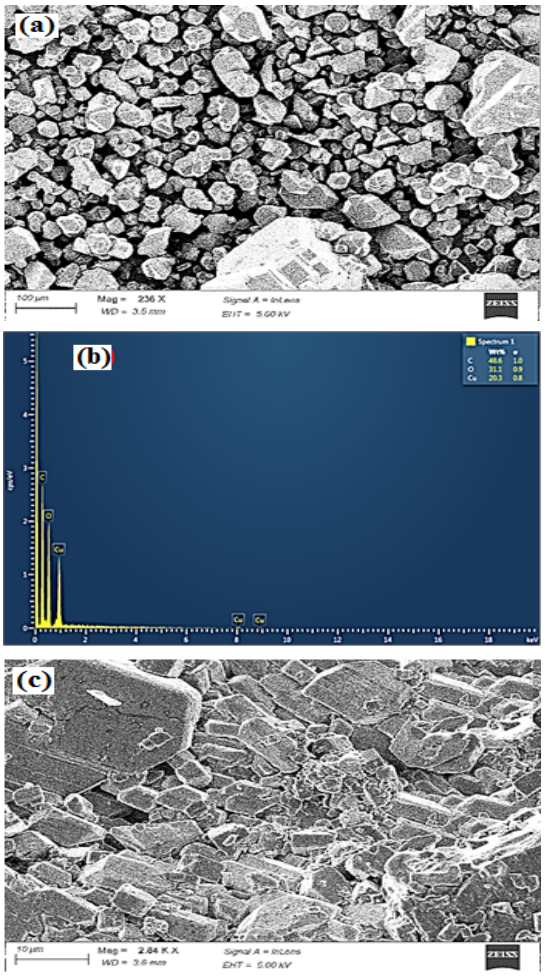

Fig. 2. (a) SEM image and (b) EDAX spectrum of Cu-MOF & (c) SEM image of 0.5S-Cu-MOF

Thermo-Gravimetric analysis

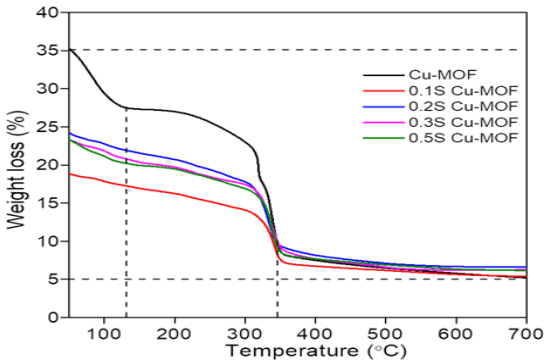

Fig. 3. TGA curve of (a) Cu-MOF, (b) 0.1S-Cu-MOF, (c) 0.2S-Cu-MOF, (d) 0.3S-Cu-MOF, (e) 0.5S-Cu-MOF

The thermal stability of parent Cu-MOF is understood from its TGA analysis studied by subjecting the sample to heating from 25°C to 700°C under N_2 flow (Fig. 3). The thermogram clearly shows ~8% weight loss up to 110°C from ambient temperature in first stage. This is due to the loss of physisorbed molecules of water and the organic solvents used in the synthesis process. While a second stage ~20% reduction in weight from 200–350°C is accounted to the loss of organic linker molecules and a final weight loss of 9% above 320°C indicative of the burial of organic linkers upon decomposition of the material[55]. And ~26.5% of total weight loss is reported to a probable phase transformation of Cu_2O to CuO which correlates to the presence of Cu_2O and CuO phases in XRD profiles. The 17.2% weight loss recorded in this analysis is due to the entire coordinated water molecules that is in agreement with the 16.2% estimated weight loss of water molecules reported[55]. The sulphated Cu-MOF showed a major weight loss of ~20 % above 110°C till 350°C. A initial weight loss below 110°C is quiet low as the physisorbed molecules are already lost during the impregnation of sulphate which involves oven drying at 100°C. The thermograms of the sulphated Cu-MOFs resembled the parent Cu-MOF above 320°C in the final stages of weight loss indicating the similar behaviour and stability of the sulphated catalysts as that of the parent MOF.

FT-IR Spectral Results

FT-IR analysis adds up to the understanding of molecular characteristics of Cu-MOF with respect to various vibrational modes of the bonds and functional groups present in the MOF structure. The bending and stretching vibrational bands[56] (Fig. 4) of Cu–O are observed at 480 and 720 cm^{-1}. The peaks observed from 800–1150 cm^{-1} are due to the various stretching vibrations of O–C=O and C–O while the deformation modes of the phenyl ring can be seen as less intense peaks between 660–760 cm^{-1}. Further, the strong vibrational modes due to carboxylic acid group of Cu-BTC are noticed at 1375, 1432 and 1625 cm^{-1}. Stretching vibrations due to OSO_3H- and asymmetric stretching of the S=O were reported to appear at 580 and 883 cm^{-1} and, 1288 cm^{-1} respectively[57,58]. However, with the vibrational of the BTC being very close in the same region, these peaks are not distinguished clearly in the spectra of sulphated Cu-BTC MOFs.

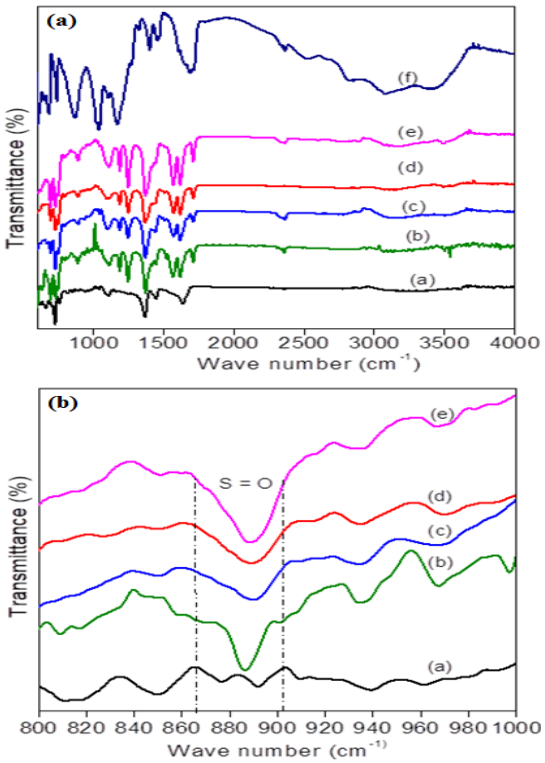

Fig. 4. FT-IR spectra of sulphated Cu-MOF (a) 0.1S Cu-MOF, (b) 0.2S Cu-MOF, (c) 0.3S Cu-MOF, (d) 0.5S Cu-MOF, (e) 1S Cu-MOF and (f) Cu-MOF samples

Raman spectra

Raman spectrum gives further insights of Cu-BTC MOF structural features (Fig. 5).

The peaks from 200-600 cm^{-1} are corresponding to the vibrational bands linked to Cu(II) ions. Those at 200-270 cm^{-1} are the stretching vibrational bands of Cu–Cu and Cu–O. The 'O' in Cu-O is from the H_2O adsorbed on Cu^{2+} ions[59]. A low intensity signal observed at 450 cm^{-1} is because of the vibrational stretching of Cu–O. Raman bands from 600-1200 cm^{-1} are commonly associated with the deformation and C-H stretching oscillations of phenyl rings in the organic linkers[59].

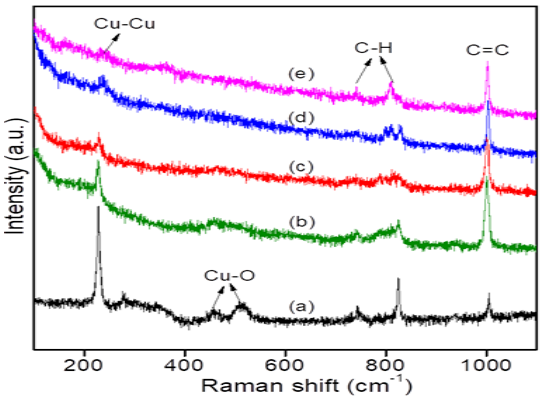

Fig. 5. Raman spectra of (a) Cu-MOF, (b) 0.1S-Cu-MOF, (c) 0.2S-Cu-MOF, (d) 0.3S-Cu-MOF, (e) 0.5S-Cu-MOF

Acidity Measurements from Ex-Situ Py-Adsorbed FTIR Studies

The Bronsted (BAS) and Lewis acid sites (LAS) present on sulphated MOF catalysts studied are measured from Py-IR spectroscopy. It is known that the vibrational signal at ~1560 cm^{-1} is due to the coordinated pyridine over BAS while the pyridine molecules adsorbed on LAS appear as a peak at ~1450 cm^{-1} [60]. The spectra (Fig. 6) of the sulphated Cu-BTC MOFs indicate higher ratio of LAS to BAS on the catalyst surface which are much higher as against the parent Cu-MOF catalyst[61]. Though Cu-BTC MOF possess very low Bronsted acidity, sulphation seems to enhance both Bronsted as well as Lewis acidity. However, the LAS outnumber the BAS, as can be observed from the $I_{Lewis}/I_{Bronsted}$ ratios obtained from the Py-adsorbed IR spectra as presented in Table 1. Synthesis of solketal from glycerol reaction is catalyzed by acid catalyst with the involvement of both Bronsted as well as Lewis acid sites reported for the selective synthesis of solketal. Enhanced acidity with increase in sulphate loading as evidenced from the Py-IR patterns justifies the increase in rate of formation of solketal with sulphate content on the surface of the catalysts.

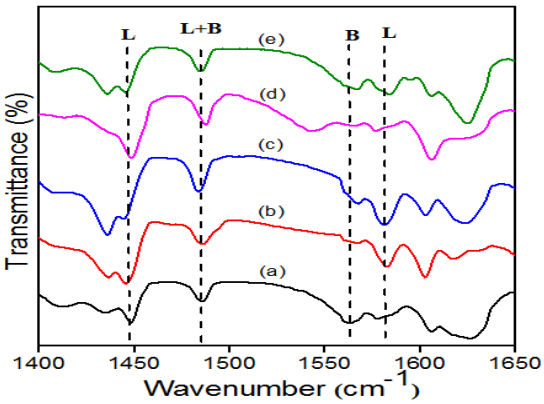

Fig. 6. Ex-situ Py-adsorbed spectra of different sulphated Cu-BTC (a) 0.0S, (b) 0.1S, (c) 0.2S, (d) 0.3S, (e) 0.5S samples

XPS analysis

The wide scan spectrum of XPS analysis of parent Cu-MOF showed (figure not given) the peaks pertaining to C 1s, Cu $2p_{1/2}$, Cu $2p_{3/2}$ and O 1s at binding energies (B.E) of 284.8, 935.5, 955.3 and 533 eV respectively. The two signals at 935.5 and 955.3 eV (Fig. 7) correspond to the B.E of Cu $2p_{1/2}$ and Cu $2p_{3/2}$ respectively of Cu(II) along with their satellite peaks at ~964.5 eV and ~942 & ~945 eV respectively[62]. The other signals at ~933.5 and ~954 eV are attributed to Cu $2p_{3/2}$ and Cu $2p_{1/2}$ in Cu(I) form. These results correlate well with the analyses from XRD and FT-IR. The O 1s XPS signal from Fig. 7c, may be split up to two at about 532.1 and 533.5 eV assigned to the presence of O^{2-} in the crystalline network[63]. The peak around a B.E. of 169 eV in case of 0.1S-Cu-MOF shifted to 170.5 eV as the loading of sulphate increased from 0.1 to 0.5. This peak is attributed to S 2p with in S(VI) state in the bound form[64]. A shift towards higher B.E. value with increased sulphate loading indicates strong interaction of the sulphate with the surface moieties of Cu-MOF. The increase in intensity of this peak with sulphate loading is clear in the Fig. 7(d). The C 1s peaks at 284.5, 286 and 289 eV can be ascribed to the –OH, C=O and O=C–OH groups respectively of the BTC linker[63].

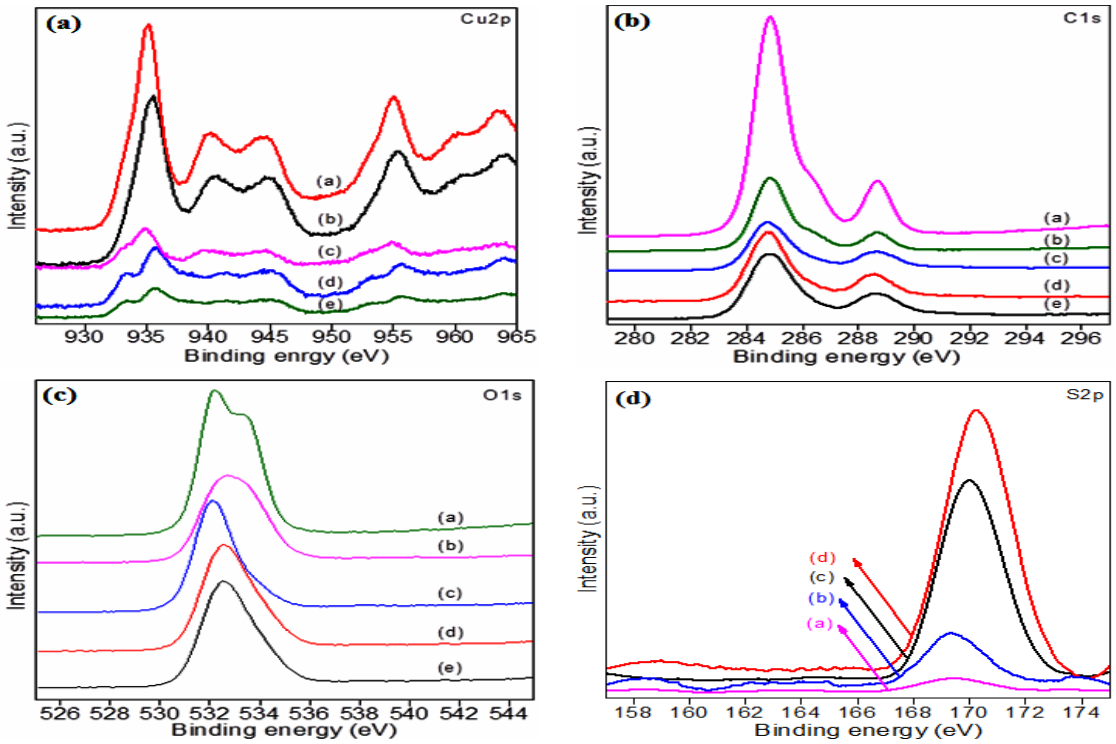

Fig. 7. X-ray photoelectron spectra of (a) Cu 2p, (b) C 1s (c) O 1s and (d) S 2p of the sulphated Cu-BTC MOF catalysts

Glycerol acetalization activity results

Glycerol acetalization using acetone was carried out over parent Cu-BTC MOF along with the various amounts of sulphate loaded Cu-BTC MOF under ambient conditions of room temperature and atmospheric pressure. A simple test was also conducted without using any amount of catalyst as well, which showed no conversion of glycerol in this blank reaction. This clearly establishes the role of the Cu-MOF or sulphated Cu-MOF in the acetalization of glycerol to solketal. The parent Cu-MOF showed about 45% conversion of glycerol and 92% selectivity towards solketal formation ascribed to the presence of LAS on the parent Cu-MOF catalyst. The acidity of the Cu-MOF was raised with the surface incorporation of sulphate group that resulted in enhanced activity both in terms of the glycerol conversion as well as selectivity to solketal formation. There was a clear increase in the conversion of glycerol/rate of formation of solketal up to 0.5S loading as shown in the Fig. 8 and there after a decrease in the conversion was observed owing to loss of activity of the catalyst with higher sulphate loading probably resulting in the burial of active sites on the surface of Cu-MOF or destabilization of the MOF structure. Hence, Cu-MOF with 0.5S loading is chosen as the optimum catalyst for obtaining better yields of solketal at ambient conditions of reaction.

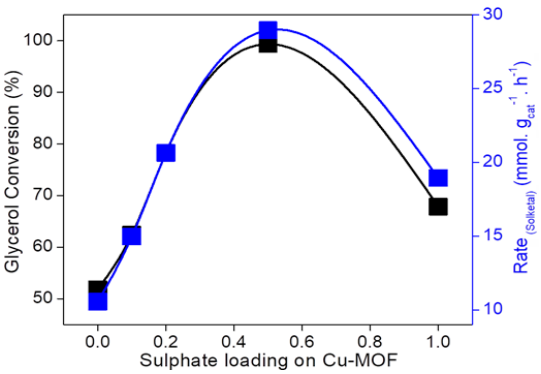

Fig. 8. Effect of sulphate loading on the acetalization activity of Cu-MOF

This catalyst is chosen to study the effect of glycerol:acetone molar ratio, time on stream and catalyst amount on the glycerol acetalization activity of the catalyst. The results are presented in figures 9a, b and c.

These results indicated (Fig. 9a) a glycerol:acetone of 1:10 (mole ratio) to show highest conversion of glycerol and hence higher yield of

solketal among the various other ratios studied. Solketal formation from acetalization of glycerol produces water as a by-product that creates a thermodynamic and a kinetic barrier for obtaining higher conversion of glycerol. The best measure to break this barrier is by taking excess acetone that can shift the equilibrium towards formation of solketal as the glycerol acetalization equilibrium constant is low[44]. Further it was also reported that acetone apart from being the acetalizing agent, can be an entrainer for the system as well. Hence, optimum glycerol: acetone molar ratio of 1:10 was taken to achieve maximum yield of solketal. The conversion of glycerol increased till 4 wt.% of catalyst taken (Fig. 9b) and above that there was no significant raise in the conversion levels. However, the selectivity to solketal enhanced with increased amount of catalyst taken which may be credited to the availability of greater no. of acid sites for the catalytic process. The other product which was obtained is identified as the 6-membered ring product i.e., the acetal that is possible through a side reaction in the acetalization process[65]. Therefore 3wt.% of catalyst is taken as optimum catalyst amount to obtain increased yields of solketal. The time on stream studies depicted in Fig. 9c indicate a steady state conversion obtained after 180 minute of the reaction time over all the catalysts studied. The rate of solketal formation was hence with calculated at 180 minute of conversion of glycerol at ambient conditions of reaction. A maximum rate of solketal formation of 29 mmol g_{cat}^{-1} h^{-1} was observed over 0.5S loaded Cu-MOF catalyst which is nearly 3 times higher when compared that over Cu-MOF which obviously establishes the role of Lewis acid sites that were enhanced with sulphation over Cu-MOF observed from the ex-situ Py-adsorbed IR studies.

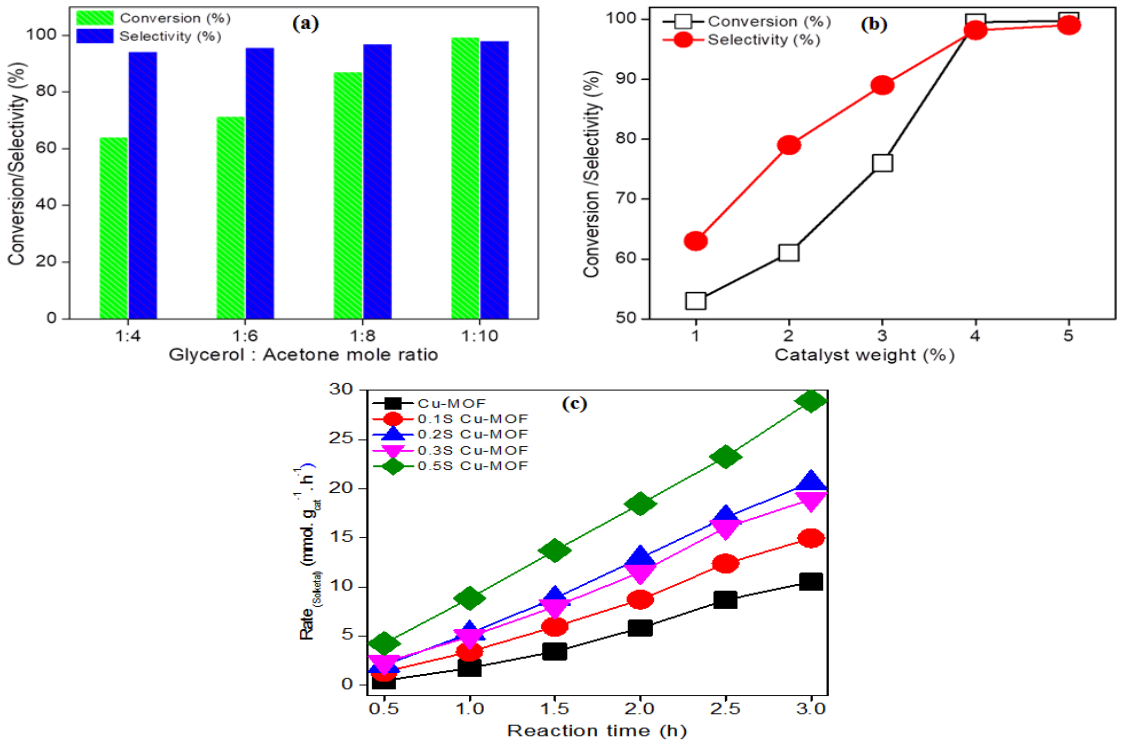

Fig. 9. Effect of (a) Gly: Ace mole ratio (b) Catalyst amount glycerol acetalization over 0.5S-Cu-MOF and (c) Time on stream activity of 0.1 to 0.5 S-Cu-MOF catalysts

Reusability studies

The reusability studies (Fig. 10) carried out for 5 cycles of reaction run over the best catalyst in the study i.e., 0.5S-Cu-MOF indicate the stable activity of the catalyst even after 5 times of use in the reaction with a very small detriment in the conversion of glycerol. The characterization studies viz., XRD, SEM-EDAX and CHNS analysis (Fig. 11, 12 and Table 2) clearly depict the catalyst to be stable after 5 cycles of reaction run, structure remaining intact and the sulphur content is also not varied much as established from EDAX and CHNS analyses for both fresh and the used catalyst.

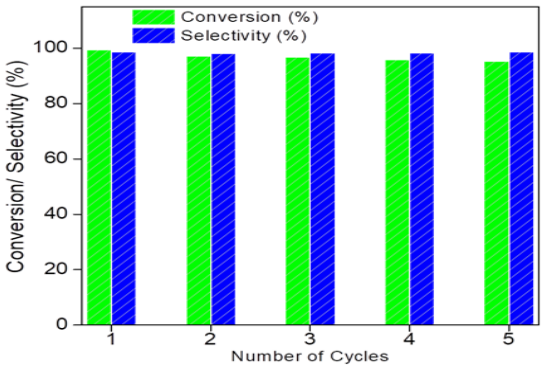

Fig. 10. Reusability of 0.5S Cu-MOF catalyst

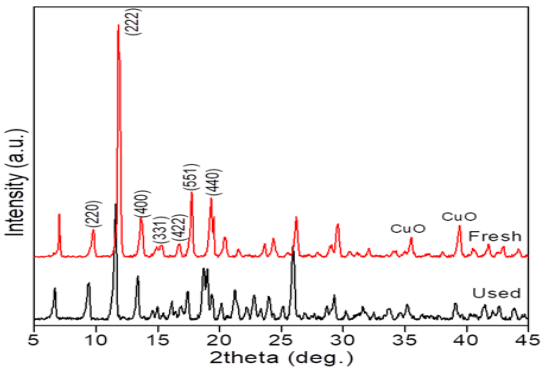

Fig. 11. XRD patterns of fresh and used (after 5 cycles of reaction run) 0.5S-Cu-MOF

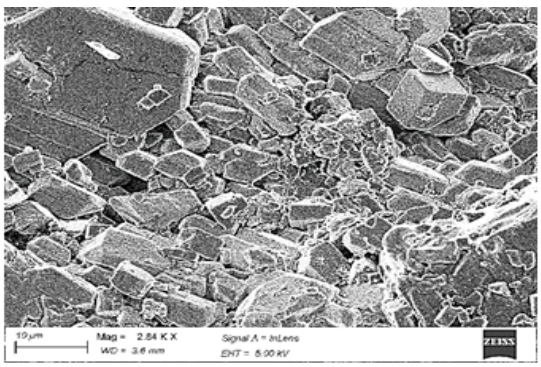

Fig. 12. SEM image of the used 0.5S Cu-MOF catalyst

Table 2: CHNS Analysis of Cu-MOF catalysts

Catalyst	Sulphur(%)	Carbon(%)	Hydrogen(%)	Nitrogen(%)
Cu-MOF	0	30.96	4.55	3.63
0.1S Cu-MOF	1.06	29.28	3.603	1.93
0.2S Cu-MOF	1.98	30.27	3.018	2.49
0.3S Cu-MOF	4.62	27.83	3.672	1.32
0.5S Cu-MOF	6.54	27.13	3.922	1.75
0.5S Cu-MOF (used)	6.23	28.47	3.52	1.68

Though there was always diverse discussion on the competitive/combined role played by the two types of acid sites i.e. Lewis and Bronsted, with some authors in support of the dominant role of Bronsted sites[66] and some others have reported the Lewis sites being crucial in defining the yields of solketal formation[67,44]. Our previous studies on the solketal formation from glycerol to over sulphate modified l-MCM 41[48], Zr-MCM 41[50] and Ti-MCM 41[49] clearly established that though both Bronsted and Lewis acid sites are necessary for the solketal formation, sulphation resulted in a greater increase of Lewis acid sites as established from ex-situ Py-IR studies. A similar observation was also made in the glycerol acetalization over acidic zeolites studied[47].

The glycerol acetalization reaction is reported to follow a bimolecular Langmuir-Hinshelwood mechanism[68]. The primary step involves the protonation of carbonyl group forming a carbenium ion of short time span over a BAS while a LAS can activate the carbonyl group forming a carbenium ion. The hemiacetal intermediate formed from the carbenium ion by nucleophilic attack of the -OH, if further attacked by either the terminal hydroxyl group or the hydroxyl attached to secondary carbon results in either a desired 5-membered ring product, solketal or an undesired 6-membered ring acetal product[67]. The same has been depicted in the Scheme 2 given below over sulphate modified Cu-MOF catalysts. Our previous studies also support that the primary step requires a Bronsted site for the formation of carbenium ion and there after Lewis acid sites are responsible for the hemiacetal formation and cyclization through a dehydration step to form selectively the 5-membered cyclic product solketal which is a kinetically favoured product over the six membered cyclic acetal[69]. In this study also, Lewis acid sites seem to dominate in devising the selectivity of the product supported by the previous studies. Synergistic effect of the structural features with tunable properties of MOF on its glycerol acetalization activity further makes these materials stand out as unique, highly potential, stable and selective catalysts for the synthesis of solketal from glycerol.

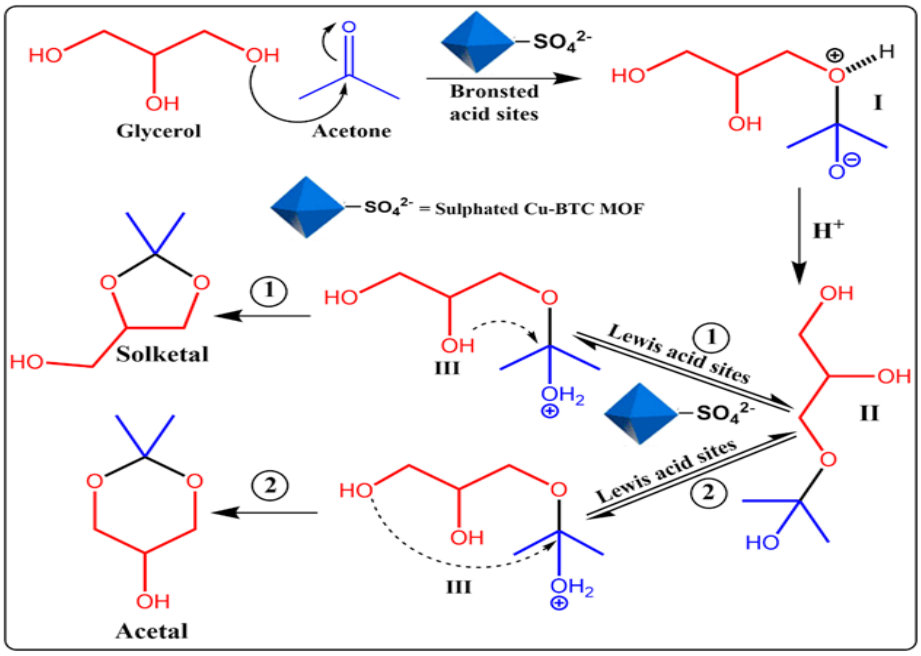

Scheme 2. Probable mechanism of glycerol acetalization over sulphated Cu-MOF

CONCLUSION

Cu-BTC MOF was synthesized by a simple solvo-thermal method and modified to enhance its acidity by sulphation using sulphuric acid through impregnation. A series of sulphated Cu-BTC MOF catalysts were prepared by variable amounts of sulphate loading taken ranging from 0.1-1 S. These series of sulphated Cu-MOF catalysts along with the parent Cu-BTC MOF were thoroughly characterized by different techniques viz., XRD, TGA, BET-surface area, FT-IR, Raman, SEM-EDAX, XPS and Ex-situ Py-IR. The analyses clearly indicated the established crystalline Cu-MOF structure remaining intact after sulphonation and the characteristic morphology of cubic and cubo-octahedral particles of Cu-MOF were noticed from SEM followed by EDAX analysis showing the desired elemental composition of Cu, O, C and S. The FT-IR and Raman studies showed the characteristics vibrational modes corresponding to the hydroxyl, carboxylate groups along with the Cu-O modes and stretching modes of vibrations of sulphate group. BET-surface resulted in a high surface and pore volume of the parent Cu-MOF while sulphation reducing the surface area owing to the closure of the pores and voids present in the structure of MOF. The XPS studies showed the presence of Cu in Cu(I) and Cu(II) forms with high surface sulphur present on the catalyst. Further, the C 1s spectra clearly established the presence of carboxylate linkers. The activity studies showed the beneficial role of sulphation in escalating the yields of the desired product, solketal through acetalization of glycerol that was achieved at ambient conditions of temperature and pressure. The other reaction parameters such as glycerol: acetone mole ratio, catalyst loading and time on stream studies to achieve optimum conversion of glycerol and higher selectivity of solketal were also established. The catalysts were found to be stable enough after 5 cycles of reaction runs without much loss in the activity. The characterization studies of XRD, SEM-EDAX and CHNS analysis supported these findings in establishing the stability of the catalysts. Enhanced acidity on the result of sulphation over Cu-MOF probably is the key factor observed over the sulphated Cu-MOF catalysts. MOFs with their high surface area, stability and vast tunability character place them ahead of their counterparts. It can be suggested from these studies that sulphated Cu-MOFs can be highly promising catalysts for the valorization of bio-glycerol to solketal.

ACKNOWLEDGEMENT

The authors express their gratitude to Dr. A. Venugopal, Chief Scientist, CSIR-IICT for his support with some of the characterization investigations.

Conflicts of interest

The authors declare no conflicts of interest.

REFERENCES

1. Furukawa, H.; Cordova, K.E.; O'Keeffe, M.; Yaghi, O.M., *Science.*, **2013**, *341*, 1230444.
2. Silva, P.; Vilela, S.M.F.; Tome, J.P.C.; Almeida Paz, F.A., *Chem. Soc. Rev.*, **2015**, *44*, 6774-6803.
3. Yap, M.H.; Fow, K.L.; Chen, G.Z., *Green Energy Environ.*, **2017**, *2*, 218–245.
4. Hsu, S.-H.; Li, C.-T.; Chien, H.-T.; Salunkhe, R.R.; Suzuki, N.; Yamauchi, Y.; Ho, K.-C.; Wu, K.C.W., *Sci. Rep.*, **2014**, *4*, 6983.
5. Young, C.; Wang, J.; Kim, J.; Sugahara, Y.; Henzie, J.; Yamauchi, Y., *Chem. Mater.*, **2018**, *30*, 3379–3386.
6. Van Nguyen, C.; Matsagar, B.M.; Yeh, J.-Y.; Chiang, W.-H.; Wu, K.C.W., *Mol. Catal.*, **2019**, *475*, 110478.
7. Schneemann, A.; Bon, V.; Schwedler, I.; Senkovska, I.; Kaskel,S.; Fischer, R.A., *Chem. Soc. Rev.*, **2014**, *43*, 6062-6096.
8. Dhakshinamoorthy, A.; Alvaro, M.; Garcia, H., *Catal. Sci. Technol.,* **2011**, *1*, 856–867.
9. Venu, B.; Shirisha, V.; Vishali, B.; Naresh, G.; Kishore, R.; Sreedhar, I.; Venugopal, A., *New J. Chem.*, **2020**, *44*, 5972-5979.
10. Zhao, M.; Yuan, K.; Wang, Y.; Li, G.; Guo, J.; Gu, L.; Hu, W.; Zhao, H.; Tang, Z., *Nature.*, **2016**, *539*, 76–80.
11. Dhakshinamoorthy, A.; Alvaro, M.; Garcia, H., *Adv. Synth. Catal.*, **2010**, *352*, 3022–3030.
12. Cirujano, F.G.; López-Maya, E.; Rodríguez-Albelo, M.; Barea, E.; Navarro, J.A.; De Vos, D.E., *Chem Cat Chem.*, **2017**, *9*, 4019–4023.
13. Zhang, F.; Shi, J.; Jin, Y.; Fu, Y.; Zhong, Y.; Zhu, W., *Chem. Eng. J.*, **2015**, *259*, 183–190.
14. Luan, Y.; Qi, Y.; Gao, H.; Andriamitantsoa, R.S.; Zheng, N.; Wang, G., *J. Mater. Chem. A.*, **2015**, *3*, 17320–17331.
15. Llabres i Xamena, F.X.; Abad, A.; Corma, A.; Garcia, H., *J. Catal.,* **2007**, *250*, 294–298.
16. Gupta, A.K.; De, D.; Bharadwaj, P.K., *Dalton Trans.*, **2017**, *46*, 7782–7790.
17. (a) Luz, I.; Llabrés i Xamena, F.X.; Corma, A., *J. Catal.*, **2012**, *285*, 285-291; (b) Sutapa, I.W.; Palapessya, B.V.; Souhoka, F. A.; and Bandjar, A., *Trends in Sciences.,* **2024**, *21*(1), 7163.
18. Anuar, M.R.; Abdullah, A.Z., *Renew Sust Energ Rev.*, **2016**, *58*, 208–223.
19. Ambat, I.; Srivastava, V.; Sillanpää, M., *Renew Sust Energ Rev.*, **2018**, *90*, 356–369.
20. Kiss, A. A.; Bildea, C. S., *J Chem Technol Biotechnol.*, **2012**, *87*, 861–879.
21. Tan, H. W.; Aziz, A. R. A.; Aroua, M. K., *Renewable and Sustainable Energy Rev.*, **2013**, *27*, 118–127.
22. Kong, P.S.; Aroua, M, K.; Daud, W. M. A., *Renewable and Sustainable Energy Rev.*, **2016**, *63*, 533–555.
23. Ardi, M.S.; Aroua, M.K.; Hashim, N.A., *Renewable and Sustainable Energy Rev.*, **2015**, *42*, 1164–1173.
24. Leal-Duaso, A.; Pérez, P.; Mayoral, J.A.; Garciá, J.I.; Pires, E., *ACS Sustainable Chem. Eng.*, **2019**, *7*, 13004–130014.
25. Leal-Duaso, A.; Pérez, P.; Mayoral, J.A.; Pires, E.; García, J.I., *Phys. Chem. Chem. Phys.*, **2017**, *19*, 28302– 28312.
26. Velázquez, D.; Mayoral, J.; García-Peiro, J.; García, J.; Leal-Duaso, A.; Pires, E., *Molecules.*, **2018**, *23*, 1–10.
27. Monteiroa, M. R.; Kugelmeier, C. L.; Pinheiro, R.S; Batalha, M. O.; Da Silva, C. A., *Renewable and Sustainable Energy Rev.*, **2018**, *88*, 109–122.
28. Samoilov, V.O.; Maximov, A.L.; Stolonogova, T.I.; Chernysheva, E.A.; Kapustin, V.M.; Karpunina, A.O., *Fuel.*, **2019**, *249*, 486–495.
29. Ballotin, F.C.; D Silva, M.J.; Teixeira, A.P.C.; Lago, R.M., *Fuel.*, **2020**, *274*, 117799-117805.
30. Agirre, I.; Güemez, M, B.; Ugarte, A.; Requies, J.; Barrio, V.L.; Cambra, J.F.; Arias, P.L., *Fuel Processing Techol.*, **2013**, *116*, 182–188.
31. Alptekin, E.; Canakci, M., *Applied Thermal Engineering.*, **2017**, *124*, 504-509.
32. Mota, C. J. A.; Da Silva, C. X. A.; Rosenbach, N.; Costa, J.; Da Silva, F., *Energy Fuels.,* **2010**, *24*, 2733–2736.
33. Neto, A.B.S.; Oliveira, A. C.; Rodriguez-Castellón, E.; Campos, A.F.; Freire, P.T.C.; Sousa, F.F.F.; Filho, J.M.; Araujo,J.C.; Lang,R., *Catalysis Today.*, **2020**, *349*, 57-67.

34. Costa, B.O.D.; Decolatti, H. P.; Legnoverde, M. S.; Querini, C. A., *Catalysis Today*., **2017**, *289*, 222–230.
35. Sutter, M.; Silva, E. D.; Duguet, N.; Raoul, Y.; Métay, E.; Lemaire, M., *Chemical Reviews*., **2015**, *115*, 8609–8651.
36. Magar, S.; Kamble, S.; Mohanraj, G.T.; Jana, S.K.; Rode, C., *Energy Fuels*., **2017**, *31*, 12272–12277.
37. Rossa, V.; da Pessanha Y, S, P.; Díaz, G. C.; Câmara, L.D.T.; Pergher, S. B. C.; Aranda, D. A. G., *Ind. Eng. Chem. Res*., **2017**, *56*, 479–488.
38. Dmitriev, G. S.; Terekhov, A.V.; Zanaveskin, L.N.; Khadzhiev, S.N.; K. L. Zanaveskin, K.L.; Maksimov, A.L., *Russian Journal of Applied Chem*., **2016**, *89*, 1619–1624.
39. Gonçalves, M.; Rodrigues, R.; Galhardo, T. S.; Carvalho, W. A., *Fuel*., **2016**, *181*, 46–54.
40. Fatimah, I.; Sahroni, I.; Fadillah, G.; Musawwa, M. M.; Mahlia, T. M. I.; Muraza, O., *Energies*., **2019**, *12*, 2872.
41. Oguzhan, I.; Senol, Y.; Oguzkaya, A.F. Period., *Polytech. Chem. Eng*., **2016**, *61*, 144-148.
42. Cornejo, A.; Barrio, I.; Campoy, M.; Lázaro, J.; Navarrete, B., *Renewable and Sustainable Energy Rev*., **2017**, *79*, 1400-1413.
43. Rodrigues, A.; Bordado, J. C.; Santos, R. G. D., *Energies*., **2017**, *10*, 1817-52.
44. Nanda, M. R.; Zhang, Y.; Yuan, Z.; Qin, W.; Ghaziaskar, H. S.; Xu, C. C., *Renewable Sustainable Energy Rev*., **2016**, *56*, 1022–1031.
45. Guidi, S.; Noè, M.; Riello, P.; Perosa, A.; Selva, M., *Molecules*., **2016**, *21*, 657.
46. Manjunathan, P.; Sanjeev P. M.; Halgeri, A.B.; Ganapati V. S., *Journal of Molecular Catalysis A: Chemical*., **2015**, *396*, 47–54.
47. Yadaiah, S.; Venkatesham, K.; Vijayalaxmi, B.; Balakrishna, M.; Sasikumar, B.; Hari Padmasri, A., *IOSR Journal of Applied Chemistry (IOSR-JAC)*., **2023**, *16*, Ser. I ,05-13.
48. Balakrishna, M.; Sasikumar, B.; Srinivas, B.; Sarma, A. V. S., Hari Padmasri, A., *Microporous and Mesoporous Materials*., **2024**, *363*, 112830.
49. Balakrishna, M.; Sasikumar, B.; Yadaiah, S.; Hari Padmasri, A., *IOSR Journal of Applied Chemistry (IOSR-JAC).,* **2023**, *16*, 01–10.
50. Balakrishna, M.; Sasikumar, B.; Srinivas, B.; Sarma, V.S. A.; Hari Padmasri, A., *Energy & Fuels*., **2024**, *38*, 21134-21143.
51. Ammaji, S.; Srinivasa Rao, G.; Chary,V.R.K., *Applied Petrochemical Research*., **2018**, *8*, 107–118.
52. Alfè, M.; Gargiulo, V.; Lisi, L.; Di Capua, R., *Materi. Chem. and Phy.,* **2014**, *147*, 744–750.
53. Yang, Y.; Shukla, P.; Wang, S.; Rudolph, V.; Chen, X.-M.; Zhu, Z., *RSC Advances*., **2013**, *3*, 17065–17072.
54. Chen, Y.; Mu, X.; Lester, E.; Wu, T., *Prog. Nat. Sci. Mater. Int*., **2018**, *28*, 584–589.
55. Schlichte,K.; Kratzke,T.; Kaskel, S., *Microporous and Mesoporous Materials.,* **2004**, *73*, 81–88.
56. Ghafuri, H.; Ganjali, F.; Hanifehnejad, P., *Chem. Proc*., **2021**, *3*, 2.
57. Wagh, K. V.; Gajengi, A. L.; Rath, D.; Parida, K. M.; Bhanage, B. M., *Mol. Catalysis*., **2018**, *452*, 46-53.
58. Selvaraj, M.; Pandurangan, A.; Seshadri, K.; Sinha, P.; Krishnasamy, V.; Lal, K. B. J. Mol. Cat. A., *Chemical*., **2003**, *192*, 153-170.
59. Dong, Z.; Mi, Z.; Shi, W.; Jiang, H.; Zheng, Y.; Yanga, K., *RSC Adv*., **2017**, *7*, 55504–55512.
60. Kno¨zinger, H.; Ratnasamy, P., *Catal. Rev*., **1978**, *17*, 31–70.
61. Krishna, V.; Naresh, G.; Kumar, V.V.; Sarkari, R.; Padmasri, A.H.; Venugopal, A., *Appl.Catal.* B., **2016**, *193*, 58–66.
62. Tang, J.; Zhang, S.; Chen, X.; Zhang, L.; Du, L.; Zhao, Q., *Catalysts*., **2023**, *13*, 956.
63. Sandra, J.; Munmun, G.; Anitha, V., *Mater. Adv*., **2024**, *5*, 3812.
64. Zhang, Z.; Yuan, H., *J Chem Technol Biotechnol*., **2020**, *95*, 2930-2942.
65. Vol'eva, V. B.; Belostotskaya, I. S.; Malkova, A. V.; Komissarova, N. L.; Kurkovskaya, L.N.; Usachev, S.V.; Makarov, G.G., *Russ J Org Chem*., **2012**, *48*, 638–641.
66. Carolina, X. A. D.; Valter, L. C. G.; Claudio, J. A. M., *Green Chem*., **2009**, *11*, 38-41.
67. Li, Li.; Tamás, I. K.; Bert, F.S.; Paolo P. P., *Green Chem*., **2012**, *14*, 1611-1619.
68. Nanda, M.R.; Yuan, Z.; Qin. W.; Ghaziaskar, H.S.; Poirier, M.-A.; Xu, C.C., *Fuel*., **2014**, *117*, 470–477.
69. Chandrasekhar, S., *Chem. Soc. Rev*., **1987**, *16*, 313-338.